Revision

14th October 2019

Effects of Dissolved Gases on Partial Anodic Passivation Phenomena at Copper Microelectrodes Immersed in Aqueous NaCl

Amelia R. Langley *[a], Philip J. Fletcher [b], Jonathan H.P. Dawes [c], and Frank Marken *[a]

[a] Department of Chemistry, University of Bath, Bath BA2 7AY, UK

[b] Materials and Chemical Characterisation Facility (MC^2), University of Bath, Bath BA2 7AY, UK

[c] Bath Institute for Mathematical Innovation, University of Bath, Bath BA2 7AY

Corresponding authors details: F.Marken@bath.ac.uk

To be submitted to Journal of Electroanalytical Chemistry
(Special issue)

Abstract

Anodic passivation for copper exposed to aqueous NaCl (model seawater) is rate limited by diffusion of a poorly soluble Cu(I) chloro species. As a result, a protective layer of CuCl forms on copper metal (with approx. 1 μm thickness) that is then put under strain at more positive applied potentials with explosive events causing current spikes and particulate product expulsion. In this report, the mechanism for this explosive film rupture and particle expulsion process is shown to occur (i) in the absence of underlying anodic gas evolution, and (ii) linked to the presence/nature of gaseous solutes. The film rupture event is proposed to be fundamentally dependent on gas bubble nucleation (triggered by the release of interfacial stress) with surface tension effects by dissolved gases affecting the current spike pattern. Oxygen O_2, hydrogen H_2, and helium He suppress current spikes and behave differently to argon Ar, nitrogen N_2, and carbon dioxide CO_2, which considerably enhance current spikes. Vacuum-degassing the electrolyte solution results in behaviour very similar to that observed in the presence of helium. The overall corrosion rate for copper microelectrodes is compared and parameters linked to passivation and corrosion processes are discussed.

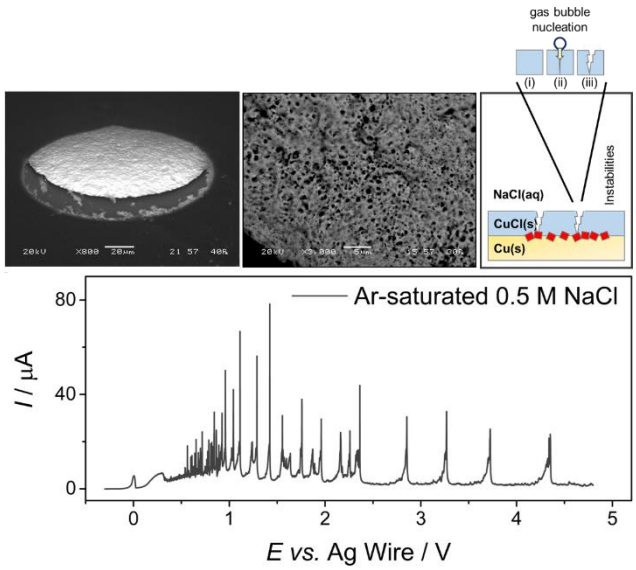

Graphical Abstract

Keywords: Electrochemistry, Passivation, Copper, Dissolved gas, Stochastic, Colloid

1. Introduction

Copper is known to be resistant to atmospheric corrosion due to the formation of patina [1,2]. In contrast, in marine environments copper (for example as the conductor in cables) corrodes significantly [2,3]. Such drastic changes in corrosion resistance are explained by the presence of chloride ions Cl^-, in marine environments (as a major component of seawater; approx. 0.5 to 0.6 M NaCl), known for its aggressive corrosive behavior towards metals.

The fundamental understanding of the copper corrosion and anodic passivation mechanisms in marine environments are important to developing effective corrosion inhibition/control processes. The copper corrosion mechanism in chloride-containing environments has been widely studied by electrochemistry to investigate corrosion product formation and the effects of altering pH, temperature, and salinity [4–8]. It is possible to consider lowering anodic overpotentials (which are well-studied) but also exploiting more partial passivation and corrosion processes at higher anodic overpotentials (which are addressed here).

Corrosion prevention is usually linked to sacrificial electrodes and cathodic protection, but an alternative strategy can be based on anodic passivation in cases in which protective passive films can be grown. Passive films have been grown on copper during anodic passivation in a variety of environments such as phosphate- [9–11], carbonate- [12–14], and chloride-containing [12,15–18] media. Copper corrosion processes during anodic passivation are complex, and passive films can be susceptible to breakdown, caused by a variety of variables including anodic potential [19], point defects [20] and anion vacancies in the passive films [21,22]. Here, we are interested in the CuCl passive film formed in model seawater at high anodic overpotentials.

More specifically, we are interested in the dynamic electrochemical behaviour observed for copper metal electrodes in neutral chloride-containing media, where both periodic [23] and stochastic [8] corrosion phenomena have been observed during anodic polarization. Interestingly, periodic phenomena have also been observed for copper in acidic chloride media [23–29], in acetate [30], and in phosphoric acid media [31], using stationary electrodes or using hydrodynamic conditions (at a rotating disk electrode). Such current oscillations and noise during anodic polarization in chloride-containing media have been explained and modelled based on the competing growth (Reaction 1) and dissolution (Reaction 2) of a film of CuCl in neutral chloride-containing electrolytes.

$$Cu(s) + Cl^-(aq) \rightleftharpoons CuCl(s) + e^- \qquad \textbf{\textit{Reaction 1}}$$

$$CuCl(s) + Cl^-(aq) \rightleftharpoons CuCl_2^-(aq) \qquad \textbf{\textit{Reaction 2}}$$

Fig. 1 gives a schematic of the hypothesised copper corrosion mechanism during anodic polarisation conditions presented in this study. Fig. 1a depicts the formation of the kinetically favoured, insoluble CuCl film, which partially passivates the Cu surface at potentials >−0.11 V vs. SCE. Although schematically depicted as dense film, this film is polycrystalline and probably porous to some degree. CuCl has previously been shown by *in situ* Raman spectroscopy as the predominant corrosion product under high overpotential conditions up to +5.00 V vs. SCE in 0.5 M NaCl(aq) [8]. Following CuCl formation, Fig. 1b shows the formation of Cu(II) species (red blocks) at the Cu | CuCl interface, postulated to occur at approximately +0.14 V vs. SCE [8].

It is the formation of Cu(II) that has been linked to the onset of noise seen in voltammetric data, and suggested to be linked to the breaking up of the CuCl film (see Fig. 1) [8,32]. The nature of the active Cu(II) species is yet to be shown conclusively, though we can expect the formation of a variety of copper complexes during the anodic polarisation of copper in aerated chloride media, where Cu_2O, CuO and $Cu_2Cl(OH)_3$ have also been identified [1,6,7,32,33]. When investigating

the passivation of copper with CuCl at potentials positive of +0.2 V vs. SCE, explosive events are seen as current spikes linked to the “colloidal dissolution” (Fig. 1d) of CuCl [8]. The cause and the contributing factors for these colloidal dissolution events are yet to be determined. The potential region has previously also been assigned to “pitting corrosion” [21].

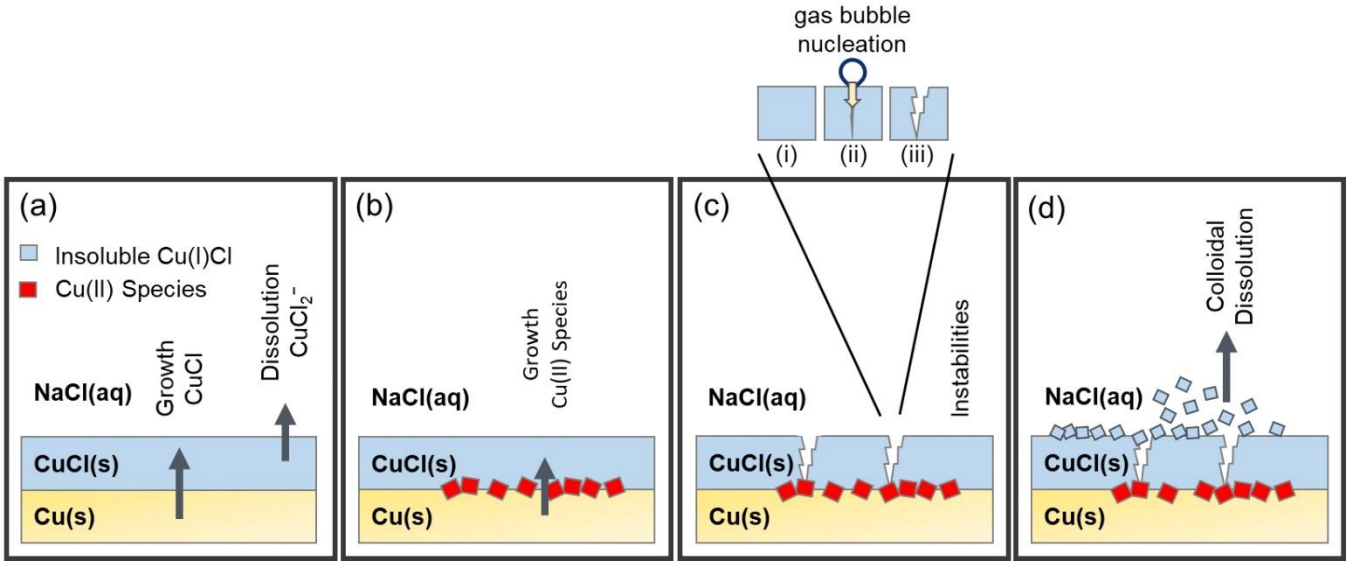

Fig. 1. *Simplified schematic drawing of (a) the growth and dissolution of polycrystalline CuCl as $CuCl_2^-$ at the surface of anodically passivated copper metal, (b) the redox driven formation of Cu(II) species at the Cu | CuCl interface, (c) the subsequent instability of the CuCl film due to Cu(II) species and bubble nucleation driven film rupture, and (d) the subsequent abrupt expulsion of colloidal CuCl* [8].

The factors that contribute to these processes are further investigated in this work where in particular, the role of dissolved gases is highlighted. The explosive “rupture” of the CuCl film is suggested to be linked to the nucleation of gas bubbles possibly linked to the sudden release of interfacial tension (see Fig. 1c). Gaseous solutes have been reported previously to significantly change the surface tension of the water | gas interface [34–36], and thereby affect bubble nucleation rates. Bubble nucleation has been reported to be relevant also in wear and tribological processes [37]. Therefore, gaseous solutes may affect the anodic passivation and corrosion of copper.

In this work, we attempt to contribute to the understanding of the dynamic passivation and corrosion processes for copper in aqueous 0.5 M NaCl. More specifically, we are interested in the corrosion mechanism in the anodic passivation potential region and in the effects of the presence/absence of dissolved gases on voltammetric responses. The results suggest that in the absence of any underlying anodic gas evolution, the abrupt break down of the passive CuCl film is strongly affected by the type/presence of gas in the aqueous electrolyte.

2. Experimental

Chemicals. All experiments were carried out at room temperature (20 ± 2 °C) and in aqueous NaCl electrolyte (0.05 M, 0.10 M, 0.50 M, or 1.00 M). Aqueous 0.5 M NaCl was used to simulate seawater conditions. NaCl (Sigma-Aldrich, >99.9% purity) and deionized water (Millipore, 18.2 MΩ cm) were used to prepare the solutions.

Instrumentation. A three-electrode (reference, counter, and working electrode) system was employed with a saturated calomel electrode (SCE) or a Ag wire pseudo-reference electrode, an epoxy-mounted Cu disc working microelectrode (25, 50, 125 and 150 µm nominal diameter), and Pt wire counter electrode. An Autolab potentiostat (µAutolab Type III, Metrohm) and GPES software were used for all electrochemical measurements. An Ivium Compactstat system (Ivium, Netherlands) was employed for bipotentiostat experiments where a second working electrode was required. Voltammetry experiments were performed from the open circuit potential (OCP) at approx. −0.25 V vs. SCE to +5.00 V vs. SCE at a scan rate of 5 mV s^{-1} (with 1 mV steps).

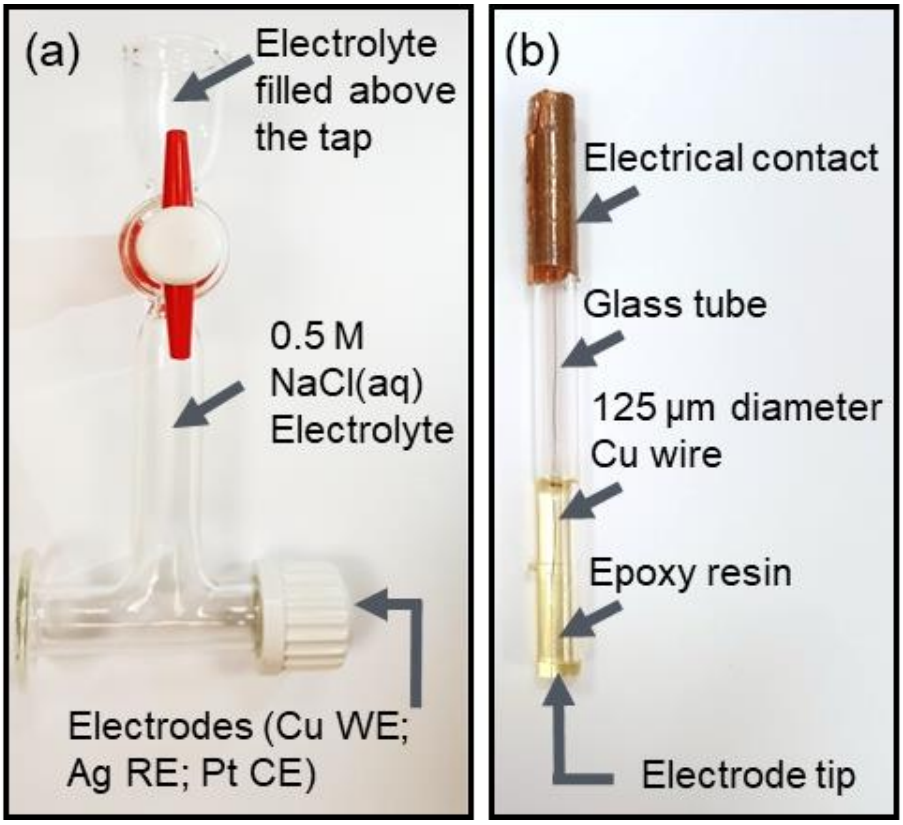

Fig. 2 *(a) Photograph of the three-electrode electrochemical cell (working electrode (WE), reference electrode (RE) and counter electrode (CE)) for the preparation of degassed electrolyte. (b) Labelled photograph of a 125 µm nominal diameter copper wire mounted in a glass tube with epoxy.*

Degassing experiments required the use of a home-made glass electrochemical cell (see Fig. 2a) with a tap to allow for gas removal under vacuum. The cell was filled with electrolyte (0.5 M NaCl) to above the tap. Three electrodes (Cu working electrode, Pt counter electrode, Ag wire pseudo-reference electrode) were inserted through a quick-fit seal. With the tap open, the cell was placed into a vacuum chamber (Thermo Scientific Heraeus Vacutherm Oven VT6025, with a membrane pump producing approximately 100 mbar vacuum) for 1 hour at room temperature. The chamber was then quickly re-pressurized and the tap immediately closed to ensure that the gas cannot re-enter into the inner electrolyte solution. The reference electrode potential in aqueous 0.5 M NaCl for the Ag pseudo-reference was determined as +0.01 V vs. SCE.

Scanning electron microscopy (SEM) (JEOL SEM6480LV) was used for surface and recession analysis of the corroded Cu electrodes. After performing linear sweep voltammetry, the electrodes were rinsed with deionized water and sonicated in deionized water for 5 minutes to remove the corrosion product. The electrodes were then dried and placed under vacuum overnight before analysis or surface morphology and recession.

Fabrication of the Copper Microelectrodes. Four sizes of copper microelectrodes were constructed with copper microwire of nominal diameters 25 μm, 50 μm, 125 μm, and 150 μm (see Fig 2b). The microelectrodes were assembled by threading the copper microwire (ADVENT Materials, 99.90% purity) through a glass tube (5 mm outer diameter), and immobilizing the wire with a non-conducting transparent epoxy (PRESI MA2+ resin and 100 CC catalyst; 1:10 catalyst:resin by weight) by either allowing the resin to set at room temperature for 12 hours, or at 100 °C for 1 hour. The resin and metal wire were polished firstly with CarbiMet paper (Buehler, P600 and P1200) and lapping film (3M U.K.) with water to achieve a flat surface, then finished on a MicroCloth (Buehler, PSA backed) with an alumina suspension (Buehler, 1.0 μm then 0.3 μm diameter particle size). The electrode was then washed with plenty of deionised water and sonicated in deionised water to remove alumina if needed. The copper electrodes were re-polished and re-used after measurements. All electrode diameters were calibrated using SEM by imaging the polished Cu surface. Table 1 summarises the measured copper electrode diameter values.

Table 1. *Cu electrode nominal diameters and diameters (/ μm) calculated by SEM imaging clean, polished Cu electrodes*

Nominal Diameter / μm	Diameter Determined by SEM / μm
150	167 ± 2
125	132 ± 2
50	56 ± 2
25	28 ± 1

3. Results and Discussion

Effects of Salinity. Fig. 3 shows typical current-voltage (*I*-*V*) curves for a 125 µm nominal diameter copper microelectrode immersed in aqueous NaCl solution. The applied potential initially starts in the Cu(0) potential range, −0.25 V vs. SCE, and is scanned positively at a scan rate of 5 mV s^{-1} (see Fig. 3a) to +5.0 V vs. SCE. An initial oxidative peak at −0.11 V vs. SCE is observed in 1.0 M and 0.5 M NaCl reflecting the formation of an insoluble Cu(I)Cl film, which partially passivates the electrode surface. When the concentration of aqueous NaCl takes one of the lower values 0.10 or 0.05 M NaCl (see Fig. 3a), the oxidation potential shifts positively, consistent with findings by Lal and Thirsk [38] and Starosvetsky et. al. [39]. When scanning the electrode potential more positive of 0.2 V vs. SCE, a sudden change occurs where a more dynamic current response (current noise) is detected, which is associated with the breakup and re-growth of the CuCl film. The resulting colloidal CuCl particles are expelled and found later in the vicinity of the electrode deposited onto the insulator shrouding [8].

Fig. 3b shows an expanded view of the voltammetric data to approx. 0.3 V vs. SCE. With lower chloride concentration, the onset of the oxidation (marked by an asterisk "*") shifts to more positive potentials, and CuCl film formation is suppressed possibly due to the formation of another type of film, e.g. a passive oxide film. The integration of the Cu(0/I) oxidation peak (indicated by the shaded area shown for the data at 0.5 M NaCl, Fig. 3b) gives a charge of 50 µC, which implies an average film thickness of approximately 1 µm (calculated assuming a CuCl density 4.14 g cm^{-3}).

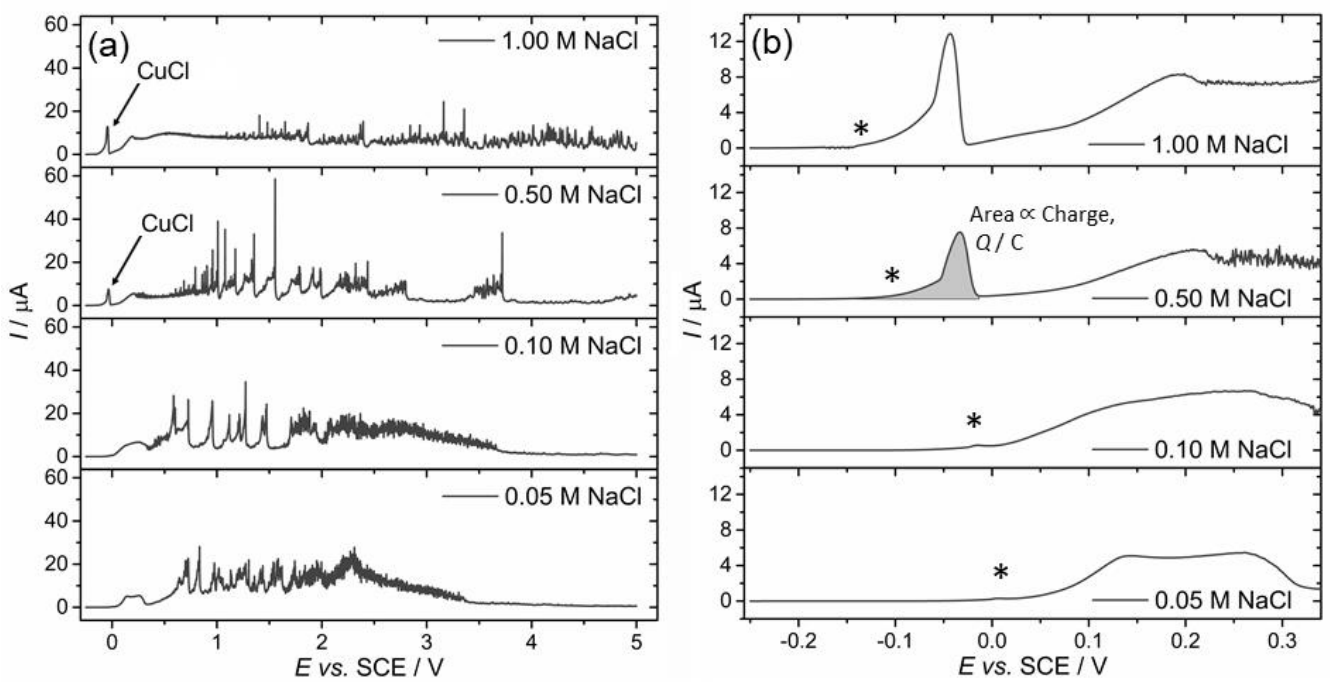

Fig. 3. *Linear sweep voltammograms (LSVs) at room temperature for a 125 µm nominal diameter copper electrode at 5 mV s^{-1} in 1.00 M, 0.50 M, 0.10 M and 0.05 M aqueous NaCl in ambient conditions from OCP at −0.25 V vs. SCE to +5.00 V vs. SCE. (a) full potential range and (b) rescaled up to 0.3 V vs. SCE. Asterisk (*) indicates the onset of copper oxidation.*

The noise features in Fig. 3a appear to be stochastic, but in fact there is a significant level of reproducibility in the position and magnitude of the spike signals as can be demonstrated by employing two copper microelectrodes simultaneously. Two identical copper electrodes of 125 µm nominal diameter were employed simultaneously in the same electrolyte solution (0.5 M NaCl) with a bipotentiostat simultaneously scanning the voltage applied to both working electrodes, WE1 and WE2 (see Fig. 4).

Perhaps surprisingly, similarities in current response between WE1 and WE2 are pronounced, indicating that the nature of these spike signals is not purely stochastic, but also voltage dependent. With physical conditions similar at both electrodes, the onset and magnitude of the “noise” signals are observed to be similar for the two electrodes in the same NaCl solution. The precise timing of individual spikes, naturally, varies. The time taken from noise onset to colloidal

dissolution characteristics (I > 20 µA) appears to be linked to both time and applied potential shown by the change in scan rate from 2 to 10 mV s^{-1} (see Fig. 4a-c).

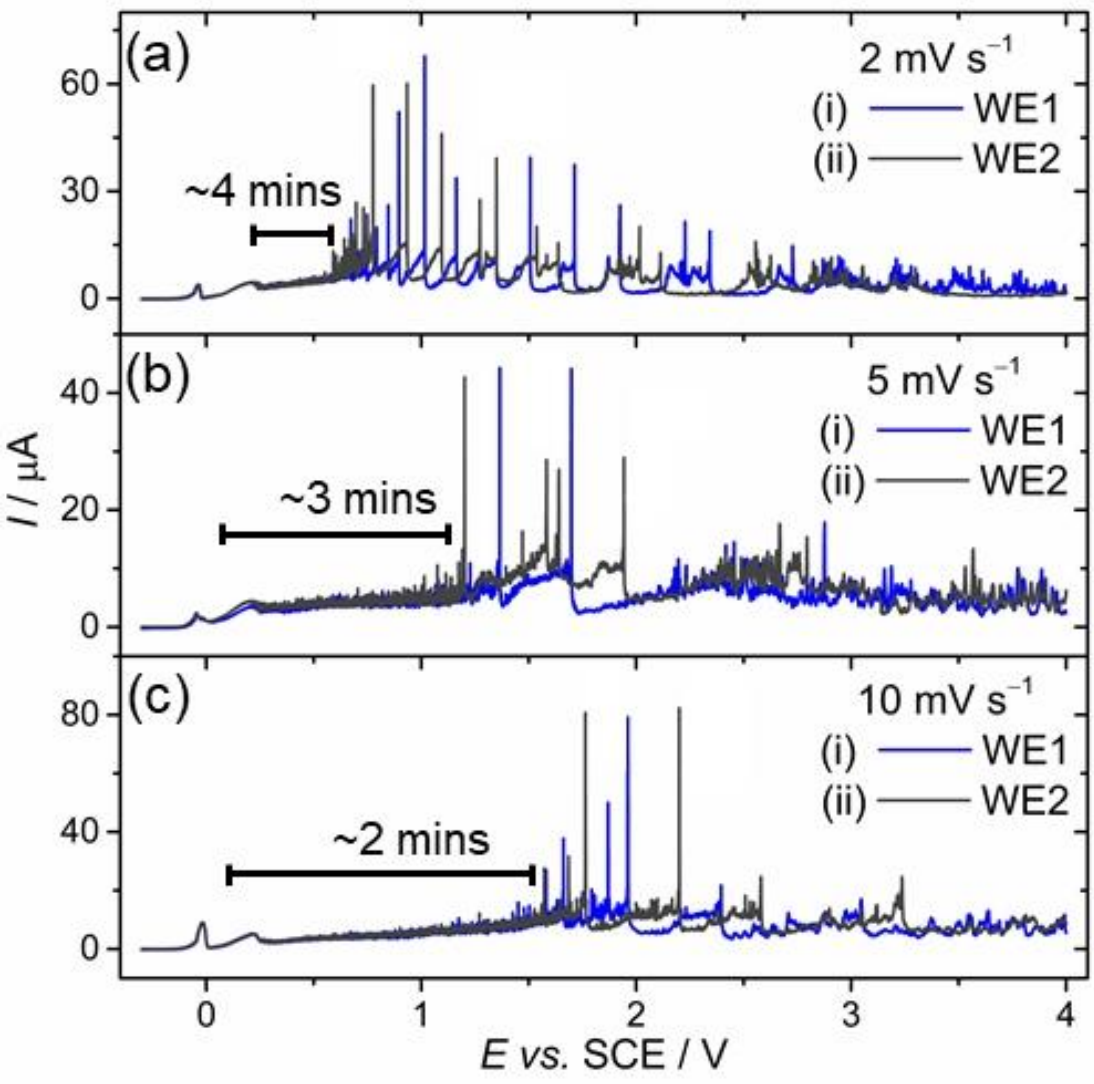

Fig. 4. *Simultaneous linear sweep voltammograms at room temperature for two identical 125 µm Cu working electrodes (WE1 and WE2) from −0.3 to +4.0 V vs. SCE in 0.5 M NaCl in ambient conditions at (a) 2 mV s^{-1}, (b) 5 mV s^{-1}, and (c) 10 mV s^{-1}*

This complex dependency of current spikes on both applied potential and time could be studied in more depth with chrono methods, but mechanistic information from this type of experimental data would be very hard to extract without further insight into the mechanism. Therefore,

additional voltammetry experiments based on solution gas content, electrode diameter, and temperature are considered next.

Effects of Degassing, De-aeration, Diameter and Temperature. With voltammetric current responses clearly reflecting the physical conditions at the electrode surface, it is interesting to explore the effects of various parameters such as electrode diameter and temperature on the current responses. The effects of inert gas were also studied by saturating the electrolyte with argon and performing voltammetry in a specially designed electrochemical cell (see Fig. 2a). To show that gas saturation was influencing the corrosion mechanism, the electrolyte was degassed using a vacuum system to contrast to the argon saturation conditions.

To explore the effects of gas on the dynamic anodic passivation for copper, linear sweep voltammetry was employed from the initial CuCl film formation (approximately −0.05 V vs. Ag wire) to more positive potential where large current spikes can be attributed to colloidal dissolution. Argon-saturation of the electrolyte leads to a visible increase in current spike events (see Fig. 5a) compared to ambient conditions. Conversely, degassing (vacuum degassing) considerably lowers current spike signals. These results point to a possible explanation based on the argon-saturation leading to enhanced bubble nucleation and subsequent film rupture, which is inhibited during linear sweep voltammetry in the degassed electrolyte. The saturation of NaCl electrolyte with air (78% N_2 and 21% O_2 [40]) resulted in an apparent dampening of current spikes. Since O_2 has an additional chemical effect on the corrosion process, this will be investigated and discussed later. First, the effects of argon saturation and degassing are investigated further with changing electrode diameter (Fig. 5).

Voltammetric data were obtained for 150, 125, 50, and 25 μm nominal diameter copper microelectrodes. The same argon-saturation effects seen for the 150 and 125 μm diameter copper electrodes (Fig. 5a-b) are also observed for the smaller 25 and 50 μm diameter copper microelectrodes (see Fig. 5c-d), where there is an increased frequency of current spikes and

thus colloidal dissolution events. The Ar-saturation effects on larger diameter electrodes (150 and 125 µm) are more pronounced compared to those at smaller electrodes (50 and 25 µm). This observation is related to the diffusional flux being higher at a smaller electrode since for a microelectrode of radius *r*, the steady state flux density is proportional to r^{-1}. One would expect the CuCl film thickness at the smaller diameter electrode to be, at least approximately, similar to that observed for larger diameters. The charge under peak 1 for electrodes with 150, 125, 50, and 25 µm nominal diameters is approximately 74, 53, 10, and 3 µC respectively, confirming similar CuCl film thicknesses (0.8-1.4 µm).

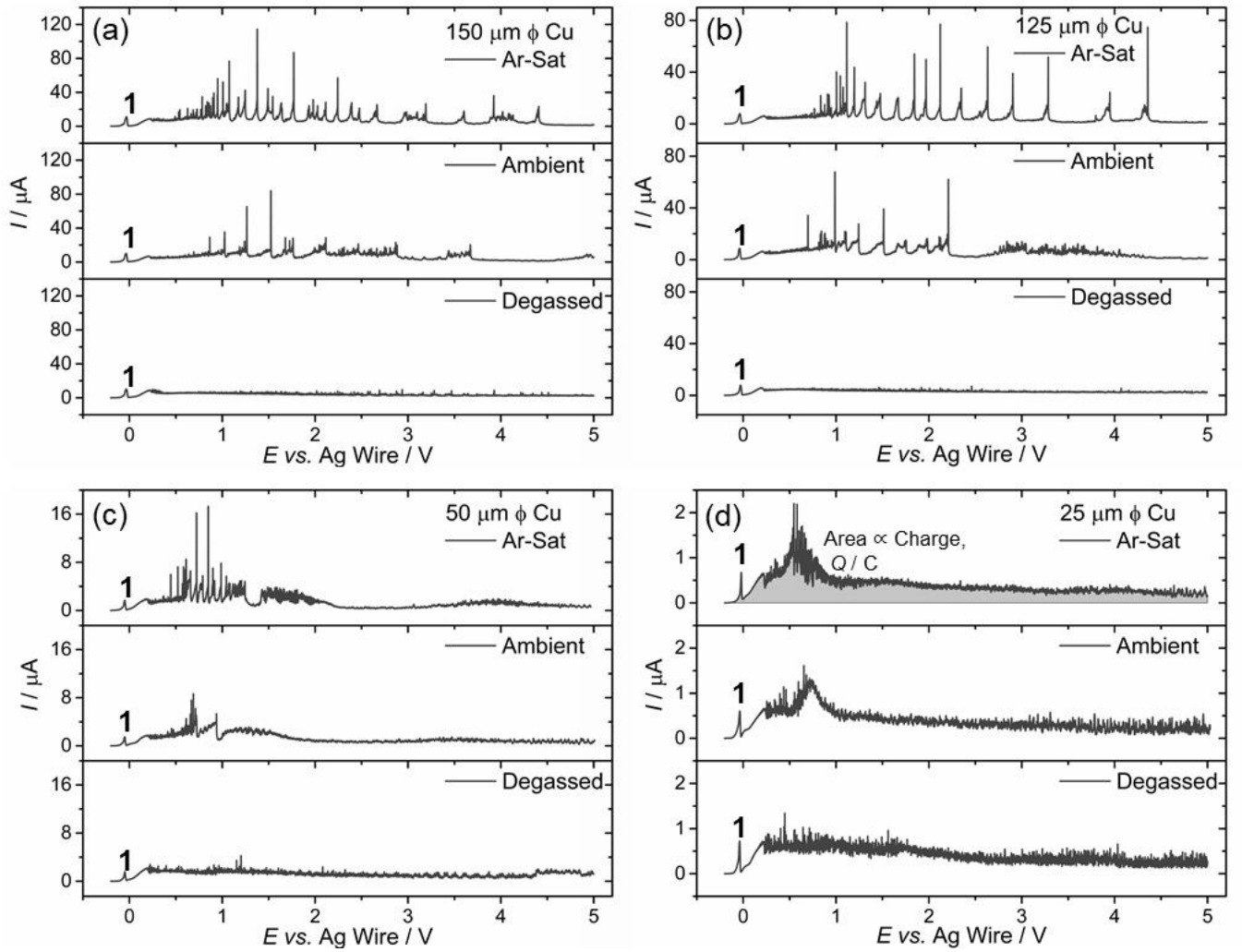

Fig. 5. *Linear sweep voltammograms at room temperature from open circuit (approx. −0.2 V) to +5.0 V* vs. *Ag wire showing the initial CuCl(s) peak 1 in Ar-saturated, ambient, and degassed 0.5 M NaCl for (a) 150 µm, (b) 125 µm, (c) 50 µm, and (d) 25 µm at 5 mV* s^{-1}*. Illustrated in (d) is the proportional relationship between the area under the voltammetric response and charge.*

To further investigate the effects of Ar-saturation and degassing of the 0.5 M NaCl(aq) electrolyte, 125 µm diameter Cu electrodes were carefully cleaned after linear sweep voltammetry in Ar-saturated, ambient and degassed 0.5 M NaCl(aq), and the corroded copper surface imaged by scanning electron microscopy (SEM). SEM images in Fig. 6 show significant morphological differences in the Cu surface when comparing degassed (Fig. 6a) and Ar-saturated (Fig. 6c) conditions. Pitting is observed for all conditions showing that pitting plays a major role in the dynamic anodic passivation mechanism for Cu in chloride-containing media. Remarkably, however, considerably more, larger pits (~800 nm diameter) are observed for the Ar-saturated sample, whereas fewer, smaller pits (~400 nm diameter) are observed for the degassed sample.

Direct anodic gas evolution is not observed during linear sweep voltammetry in Ar-saturated NaCl(aq). However, one could hypothesise with strong support from SEM imaging that gas bubbles nucleate at the corroding surface. This could be linked to very low levels of gas production or simply an increasing strain in the film and subsequently release of the strain with nucleation of a bubble. This then leads to expulsion of CuCl particulates. The formation of a crack in the CuCl film could be associated with rapid uptake of gas as viscous water would not fill the resulting crack fast enough. It is the nucleation of gas bubbles, which could in this way be contributing to the colloidal dissolution of CuCl during voltammetry (see Fig. 5).

When converting the charge Q_{total} into a theoretical recession due to dissolution of copper (copper density of 8.92 g cm^{-3} [41] and assuming a one-electron dissolution without side reactions), the rate of estimated copper recession is considerably higher for the smaller diameter electrodes (see Fig. 7a-b). This is consistent with an increased flux at smaller microelectrodes. This increase in flux is responsible for current spike features in Fig. 5c and Fig. 5d being less apparent.

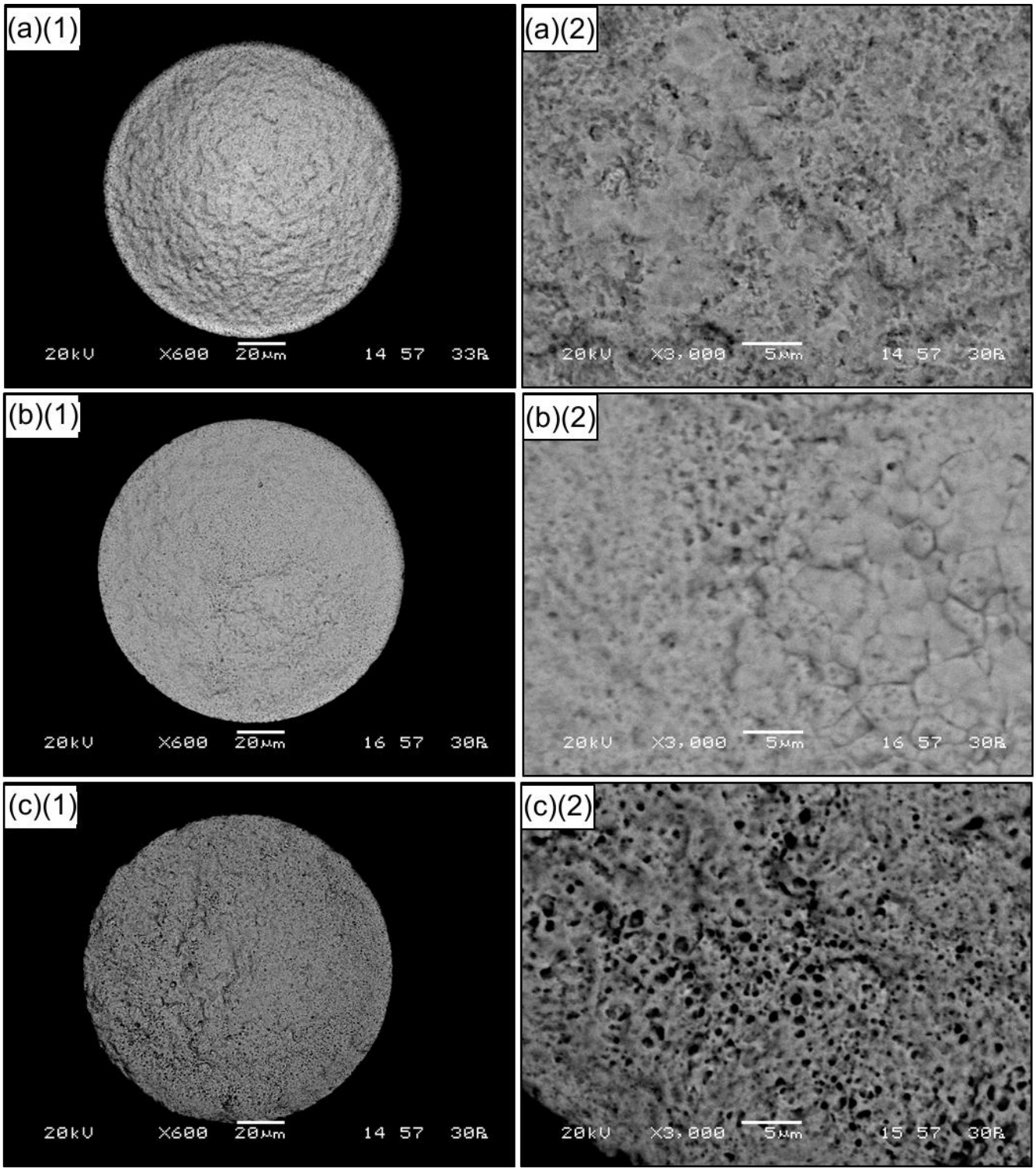

Fig. 6. *Backscattered scanning electron microscopy (SEM) images of 125 µm Cu electrodes with corrosion products removed after linear sweep voltammetry in (a) degassed, (b) ambient and (c) Ar-saturated 0.5 M NaCl(aq) at 5 mV s^{-1} from approx. −0.2 to +5.0 V vs. Ag. (1) at ×600 magnification and (2) at ×3000 magnification.*

It is interesting to compare the calculated recession effects (based on total charge) with experimental data obtained from scanning electron microscopy (SEM). Fig. 7c-e shows that the recession of a 125 μm Cu electrode after linear sweep voltammetry from −0.2 to +5.0 V vs. Ag wire (at 5 mV s^{-1}) for all three cases (Ar-saturated, ambient, and degassed solution) is indicative of a recession of 17-21 μm. This estimate contrasts with values based on electrochemical charge (see Fig. 7a-b) of 25-34 μm. Although the agreement is reasonable, there must be some additional current possibly due to generating some Cu(II). Overall, the effect of the presence of air or argon on the rate of the recession process seems minor. One important conclusion at this point is the absence of any additional currents linked to gas evolution, for example, linked to oxygen evolution. In the absence of anodic gas evolution, it seems possible that externally supplied gases could affect the processes at the corroding copper surface.

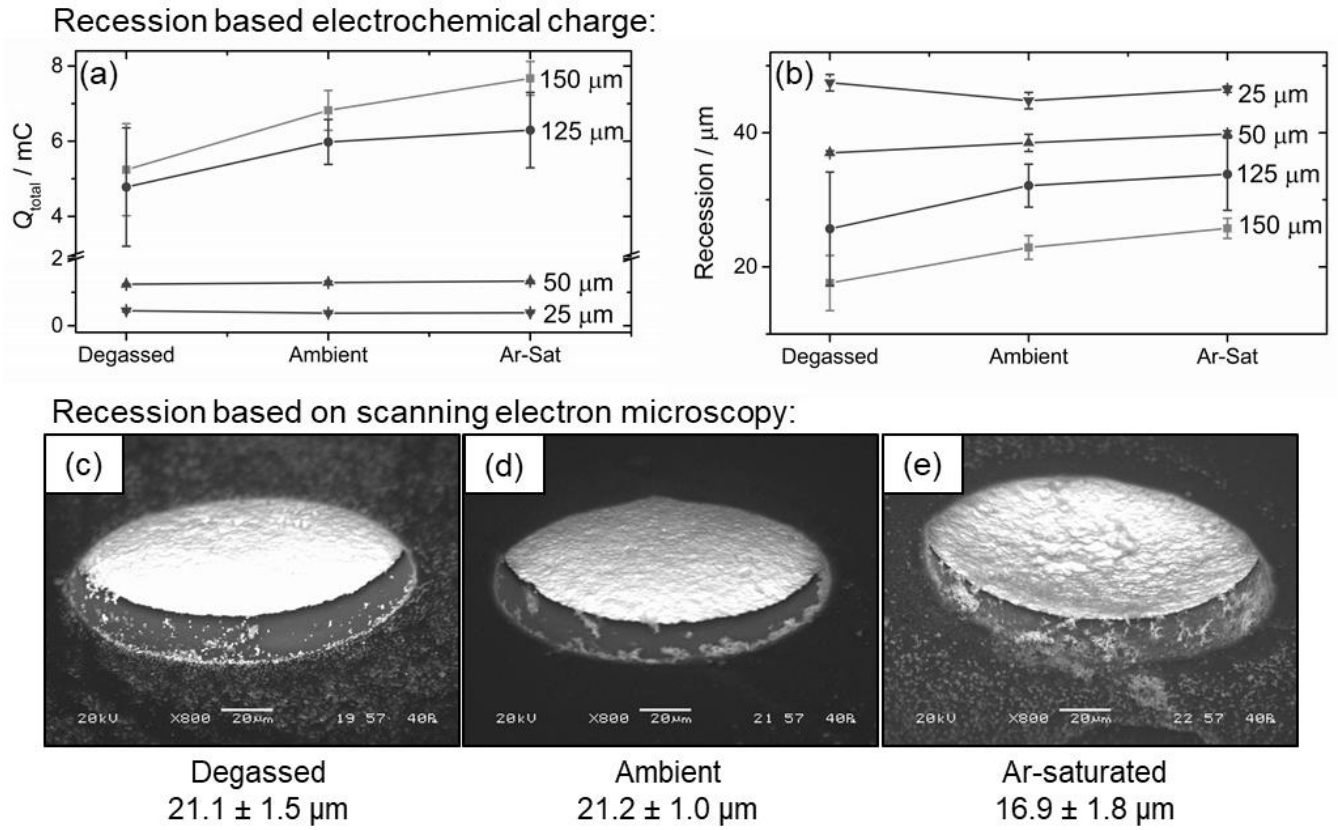

Fig. 7. *(a) total charge, Q_{total} / mC and (b) estimated electrode recession (/ μm) for 150 (■), 125(●), 50(▲), and 25 (▼) μm nominal diameter Cu microelectrodes corresponding to linear sweep voltammogram data from current responses given in Fig. 9 in degassed, ambient, and Ar-saturated 0.5 M NaCl (assuming all Cu(s) + Cl^-(aq) → CuCl(s) + 1e^-). Also shown are scanning electron microscopy (SEM) images of recessed 125 μm nominal diameter Cu electrodes after linear sweep measurements from open circuit (approx. −0.2 V vs. Ag wire) to +5.0 V vs. Ag wire*

at 5 mV s^{-1} in (c) degassed, (d) ambient, and (e) Ar-saturated 0.5 M NaCl(aq). Errors calculated from triplicate experiments.

Changes in temperature are likely to be important in affecting corrosion rates directly (via Arrhenius-type activation energies or via viscosity [42]) as well as indirectly via gas solubility [35,43].The overall effects of temperature are thus investigated for 125, 50 and 25 µm nominal diameter copper microelectrodes (Fig. 8). The voltammetry data given in Fig. 8a1-c1 show that a decrease in temperature from 23 °C to 3 °C visibly decreases the number of current spikes observed during the anodic polarisation of copper in 0.5 M NaCl(aq). More importantly, the integrated corrosion current (charge, *Q*) which directly reflects the rate of corrosion, decreases at lower temperatures. Although processes studied here are complex, it is possible to treat the integrated corrosion current as a composite process with a composite activation parameter to reveal (at least in first approximation) underlying mechanistic trends.

Temperature studies enable the calculation of an approximate composite activation energy, E_a (Fig. 8a2-c2) as per the Arrhenius equation (based on the integrated corrosion current, $Q \propto e^{-E_a/RT}$) for the overall corrosion rate averaged over these extended voltages. Data for ln*Q* versus T^{-1} is plotted in Figure 8 and the slope from the data is equal to E_a/R. Based on this, the apparent E_a for copper corrosion (typically 16 to 24 kJ mol^{-1}) is consistent with that typical for diffusion processes in aqueous media [44]. This suggests that Cu(I) is being formed at constant concentration (given by the solubility product) at the CuCl(s) | water interface and transported into the bulk solution via diffusion. This process appears to dominate in the rate of the multi-step overall reaction at these types of microelectrodes.

It is hypothesised that a slight increase in the apparent composite activation energy for the larger diameter electrodes (125 µm) could be linked to a change in the type of diffusion from more spherical to more planar diffusion with increasing electrode diameter (decreasing the flux and thereby causing a change in the composite activation energy). More work will be needed to resolve further components contributing to the activation energy.

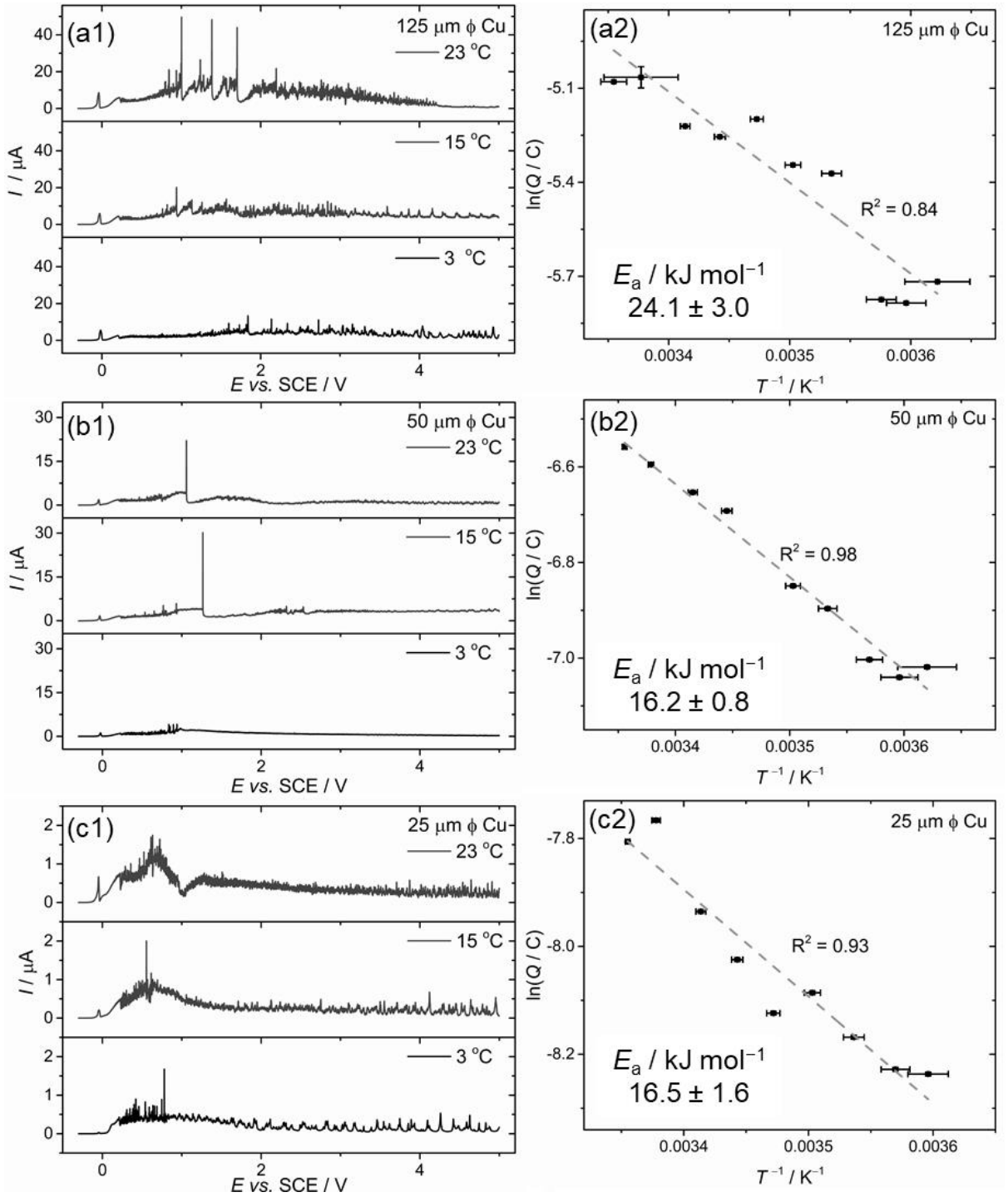

Fig. 8. *(a1-c1) Linear sweep voltammograms at 23, 15 and 3 °C from open circuit (approx.−0.3 V vs. SCE) to + 5.0 V vs. SCE at 5 mV s^{-1} in ambient 0.5 M NaCl. (a2-c2) Arrhenius plots for ln(Q / C) versus T^{-1} (/ K^{-1}) at a range of temperatures from 3 to 25 °C for (a) 125, (b) 50, and (c) 25 μm diameter (ϕ) Cu microelectrodes. Errors calculated from triplicate experiments.*

Effects of Dissolved Gases. As previously observed for Ar-saturation and degassing studies (see Fig. 5) the level of dissolved gas appeared to play a crucial role in the corrosion and passivation behaviour of the copper electrodes. The effects of Ar, air, and degassing have been mentioned previously; in this section the survey of gas effects on the copper corrosion/passivation behaviour is expanded to include He, H_2, O_2, N_2, and CO_2 (Fig. 9). It is important to consider the effects of gases present in marine environments such as CO_2 and O_2, as well as H_2 which is produced by a number of subsea processes including cathodic protection [45,46] and scale formation [46,47]. Helium was chosen to investigate the effects of an inert gas, which is commonly employed in deaeration of solutions.

Fig. 9 shows that the initial oxidation peak at approx. −0.05 V vs. Ag associated with the formation of CuCl(s) is present for all instances of gas saturation and degassing, and current "noise" is always detected. Such consistency shows that the underlying chemistry remains mostly the same, i.e. the formation of CuCl(s), dissolution of $CuCl_2^-$(aq) and the formation of strain and subsequent instabilities due to Cu(II) formation (see Fig. 1). To investigate the consistency of the initial chemistry, the approximate thicknesses of CuCl formed at −0.05 V vs. Ag for each electrolyte environment was determined, and the results are given in Table 2. For all gas-saturation scenarios and degassing other than for O_2-saturation, the estimated thickness (assuming CuCl density of 4.14 g cm^{-1}) is the same as for ambient conditions, at approx. 1 µm. O_2-saturation, however, seems to have an effect on CuCl film formation, where only a thickness of approx. 0.4 µm is calculated. This possibly indicates the formation of a CuCl film with improved passivation linked to defects or a change in grain size.

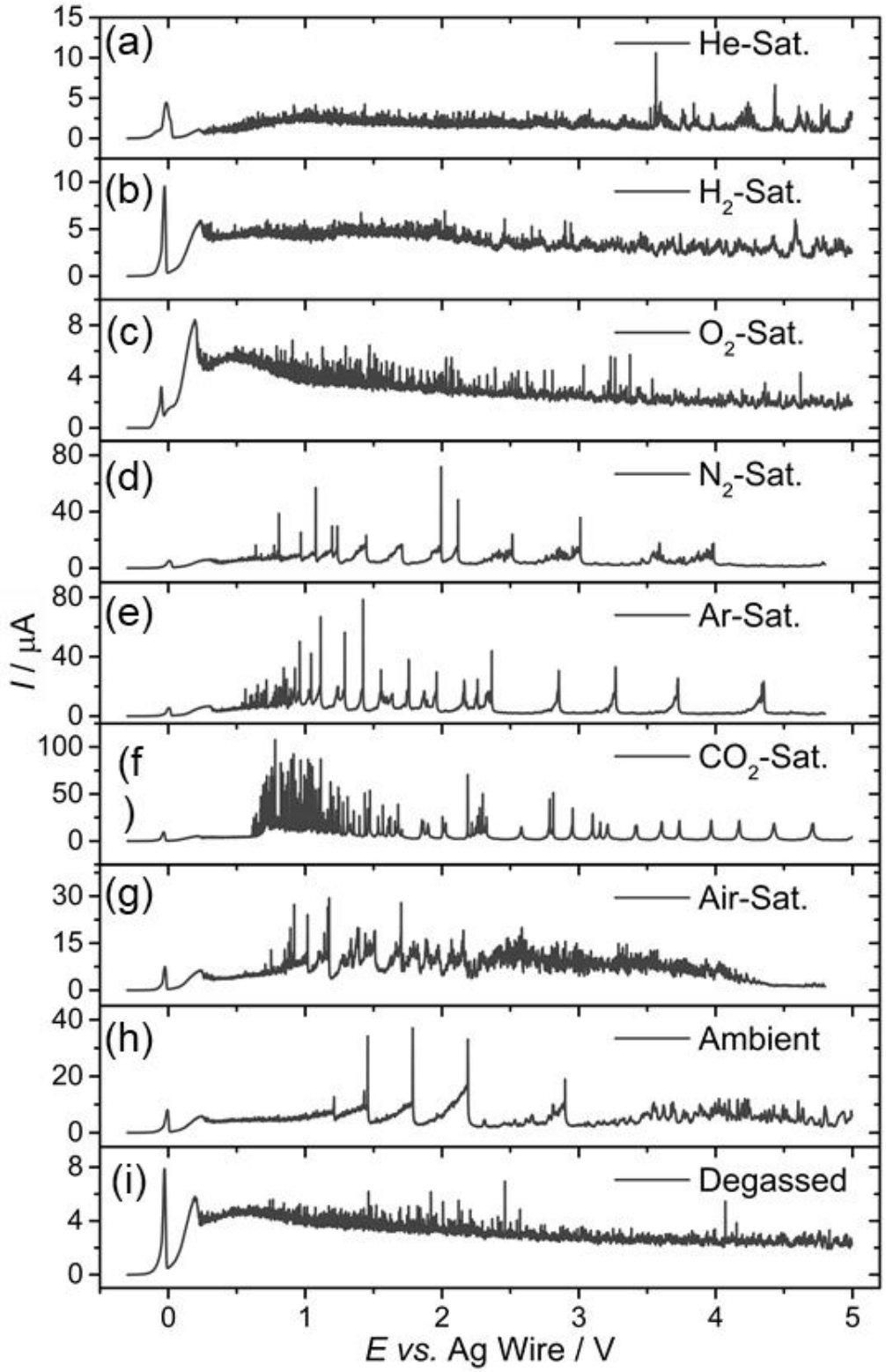

Fig. 9. *Linear sweep voltammograms at room temperature for 125 µm nominal diameter Cu microelectrode from open circuit (−0.2 V) to + 5.0 V vs. Ag wire at 5 mV s^{-1} in (a) He-saturated, (b) H_2-saturated, (c) O_2-saturated, (d) N_2-saturated, (e) Ar-saturated, (f) CO_2-saturated, (g) air-saturated, (h) ambient, and (i) degassed aqueous 0.5 M NaCl.*

Another key difference observed in all cases given in Fig. 9 is the current spikes attributed to colloidal dissolution events, which are either enhanced or suppressed compared to ambient conditions depending on the presence and type of dissolved gas. Data shown in Fig. 9a suggest that He suppresses the rupture of the CuCl film in a very similar way to the degassing of the electrolyte. Also, H_2- and O_2-saturation results in voltammetric features that seem similar. In contrast, N_2 and CO_2 (Fig. 9d and Fig. 9f, respectively) have similar effects to Ar (Fig. 9e, discussed previously), where current spike events are enhanced for all three gases compared to ambient conditions, with CO_2 having the greatest effect.

Table 2. *Calculated CuCl thickness (/ μm) from oxidation peak at −0.05 V vs. Ag in voltammetry data for He-saturated, H_2-saturated, O_2-saturated, N_2-saturated, Ar-saturated, CO_2-saturated, air-saturated, ambient, and degassed aqueous 0.5 M NaCl using the SEM determined electrode diameter (132 ± 2) μm assuming CuCl density of 4.41 g cm^{-3}. Errors are calculated from triplicate experiments.*

Gas	He	H_2	O_2	N_2	Ar	CO_2	Air	Ambient	Degassed
Film Thickness / μm	1.12 ± 0.02	1.09 ± 0.02	0.43 ± 0.02	0.88 ± 0.02	0.78 ± 0.01	1.17 ± 0.11	1.06 ± 0.03	1.02 ± 0.02	0.87 ± 0.01

Perhaps interestingly, for CO_2-saturated conditions at high applied potential, almost repetitive pulses of current bursts occur. In fact, voltammetry for N_2-, Ar- and CO_2-saturated NaCl solution exhibit current spike uniformity upwards of 3 V *vs.* Ag in 0.5 M NaCl, potentially indicative of underlying oscillatory behavior. To develop an understanding of the role of these different gases in the anodic passivation mechanism, the observed voltammetric responses will be compared to the known effect of gases on surface tension of water.

Lubetkin [48] evaluated surface tension effects of gases on aqueous electrolyte media and discussed the relevance in the nucleation kinetics of gas bubbles. The discussion by Lubetkin highlights the role of gases as surfactants, altering surface tension of water γ, in turn affecting

bubble nucleation rates J, proposing that $J \propto \exp(\gamma^3)$ [49]. The effects that different gases have on water surface tension has to be taken into consideration to understand the effect of different gases on the copper corrosion mechanism. The change in surface tension with gas pressure is denoted b (see Table 3).

Both helium and hydrogen show very small or insignificant effects on water surface tension due to a lack of molecular interaction. This could be a reason for voltammetric data for degassed and He- or H_2-saturated solution showing very similar characteristics without any bigger current spikes. The remaining noise signal positive of 0.21 V vs. Ag (0.20 V *vs.* SCE) could be linked to residual gas pressure or the pure water vapour pressure. Nitrogen and argon show enhanced current spikes with similar characteristics, in agreement with very similar values for $d\gamma/dp$ (see Table 3).

Voltammetric data for CO_2 (Fig. 9f) is rich in current spikes particularly in the potential range from 0.8 to 1.4 V vs. Ag in agreement with a much stronger effect of CO_2 on surface tension (see Table 3). However, the chemistry occurring in CO_2-saturated electrolyte could significantly differ from that in the presence of inert gas saturation. The pH could be slightly lowered due to CO_2 dissolution and this could lead to additional effects (including active participation of carbonates in passivation). In fact, in aqueous NaCl, localized variations in pH are possible and very difficult to measure or control. The effects are therefore not further considered in this report.

Table 3. *The change in aqueous surface tension with pressure, b = dγ/dp for different gases, reproduced from Massoudi and King* [34].

Gas	$b \equiv \frac{d\gamma}{d(pressure,p)}$ **/ (10^{-5} N cm^{-1} atm^{-1})**
He	0.0000
H_2	−0.0250
O_2	−0.0779
N_2	−0.0835

Ar	−0.0840
CO_2	−0.7789

The trend in current spikes can be shown quantitatively by performing a peak search above a chosen threshold for each voltammetric dataset given in Fig. 9. The threshold was determined as 3× root-mean-square (RMS) of the current signals. Fig. 10 suggests a monotonic correlation between the number of peaks above the threshold n_{peak} as a function of b.

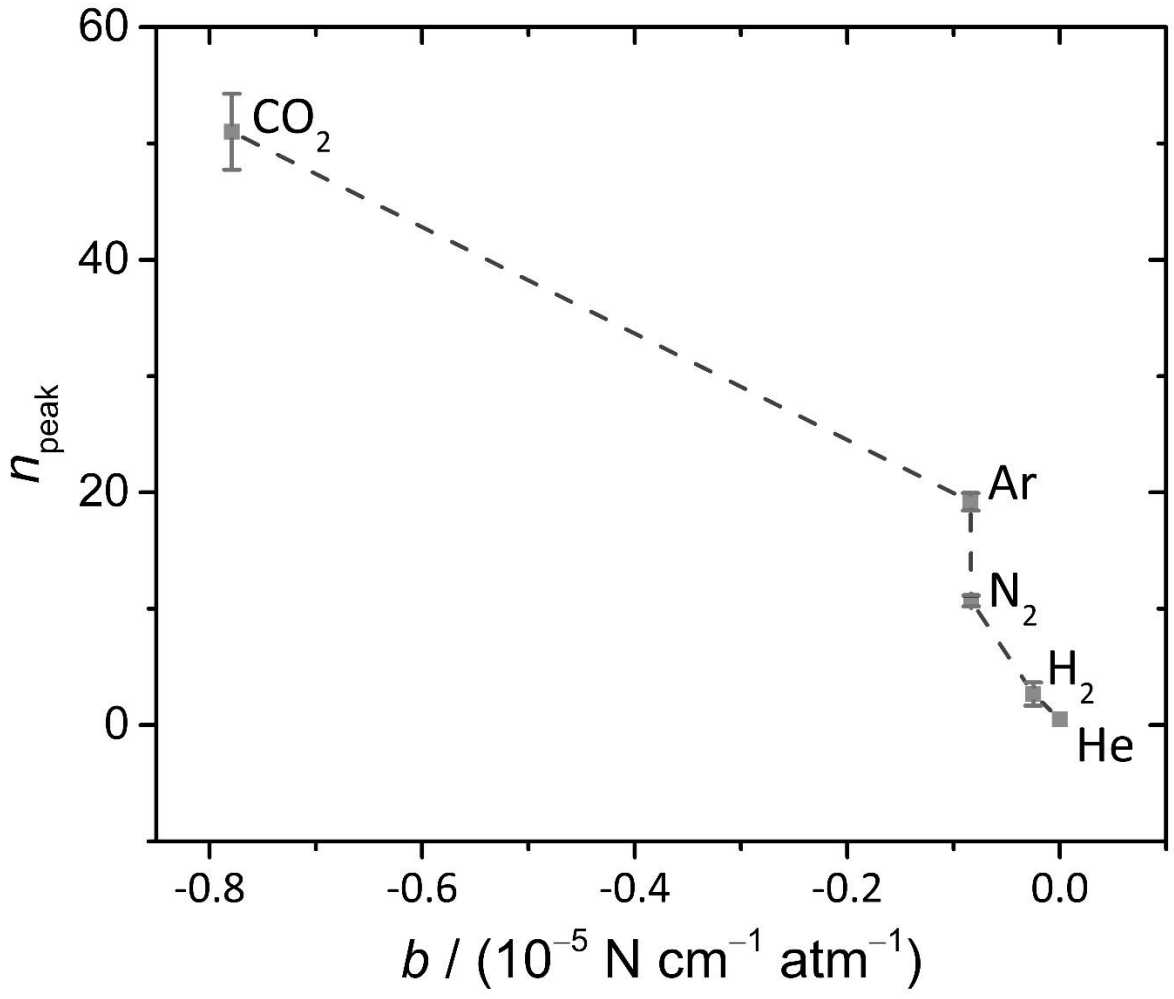

Fig. 10. *Plot of the number of current spikes n_{peak} during linear sweep voltammetry measurements in CO_2-, Ar-, N_2-, H_2- and He-saturated 0.5 M NaCl(aq) (Fig.* ***9****) as a function of b (Table 3, the ability of the chosen gas to lower surface tension). Peak search threshold = 3×RMS for each data set. Errors are calculated from triplicate experiments.*

One significant case of inconsistency of gas behaviour with data in Table 3 is that of O_2-saturation. O_2-saturation seems to result in similar current suppression effects (Fig. 9c) compared to degassing the electrolyte (current spikes remain <10 µA throughout the voltammetric sweep). One explanation could be that O_2-saturation can be assumed to have additional chemical effects on the corrosion process. Even for 20% oxygen (air-saturated electrolyte, Fig. 9g) there is a suppression effect on current spikes when compared to N_2-saturated solution. Oxygen gas is known to react with copper and various copper complexes giving insoluble copper hydroxyl-chlorides, $Cu_2(OH)_3Cl$ (via Reaction 3 and Reaction 4) [50–52]. These could affect the growth and grain structure of the CuCl film.

$$4CuCl(s) + O_2(g) + 4H_2O(l) \rightleftharpoons 2Cu_2(OH)_3Cl(s) + 2HCl(aq) \qquad \textit{Reaction 3}$$

$$2Cu(s) + O_2(g) + Cl^-(aq) + 2H_2O(l) \rightleftharpoons Cu_2(OH)_3Cl(s) + OH^-(aq) \qquad \textit{Reaction 4}$$

Since CuCl is shown to be the predominant corrosion product during anodic polarisation [8,53–55], a reaction with oxygen forming basic copper chlorides modifying the CuCl film, possibly at the grain structures of the film, could result in improved passivity (e.g. lower current spikes in voltammograms).

Table 4. *Table of calculated Cu microelectrode recession (/ µm) based on electrochemical data in linear sweep voltammograms (LSVs) from −0.2 V to +5.0 V vs. Ag wire at 5 mV s^{-1} in aqueous 0.5 M NaCl, using the SEM determined diameter (132 ± 2) µm in the calculations. Errors are calculated from triplicate experiments.*

Gas	H_2	He	O_2	CO_2	N_2	Ar	Air	Ambient	Degassed
Electrode Recession / µm	23.4 ± 3.5	9.6 ± 4.8	16.2 ± 0.5	35.6 ± 0.6	28.8 ± 3.9	32.0 ± 5.4	32.7 ± 4.0	30.9 ± 3.2	25.7 ± 8.5

Finally, it is interesting to ask whether the overall rate of corrosion (or $Q_{total} \propto$ electrode recession) is significantly affected in these different electrolyte conditions. For each voltammetric response (from −0.2 to 5 V vs. Ag at 5 mV s^{-1}) given in Fig. 9, the total charge (assuming all Cu → $Cu^+ + e^-$) and thus electrode recession of the system, has been estimated (based on a Cu density 8.96 g cm^{-1} [41]). The results are given in Table 4. The corrosion rate for O_2-saturation appears low at 16 μm compared to 23-36 μm for CO_2, H_2, Ar, and degassing (Table 4). The value for helium is even lower at 10 μm. Therefore, passivation of the CuCl film appears to be effective based on both (i) chemical reaction due to O_2-saturation and (ii) suppressed nucleation of gas bubbles for He-saturated electrolyte.

4. Conclusions

In this report, we have explored the effects of diameter, electrolyte concentration, dissolved gas levels and type, and temperature on the formation of partial passivation films on copper microlectrodes immersed in aqueous NaCl solutions. We find that salinity affects the solubility of the protective CuCl film, whereby the solubility of CuCl increases with decreasing chloride concentration, consistent with the known solubility product for CuCl. In aqueous 0.5 M NaCl a partially passive film of CuCl is formed with typically 1 μm thickness independent of the copper microelectrode diameter. However, voltammetric signals clearly reflect the changes in dissolution flux away from the smaller diameter electrodes in terms of a higher total charge per area (or a higher apparent rate of recession).

Current spikes observed during voltammetry have been linked to the sudden rupture of the passive CuCl film. Experiments with two simultaneously scanning electrodes yielded very similar current spike pattern, suggesting reproducible effects from electrolyte environment and dissolved gases. SEM studies at the corroded Cu surface showed considerable changes in morphology, where many large pits were observed for Ar-saturated conditions compared to fewer, smaller pits for degassed conditions. Such observations indicate that the large current

spikes are the result of bubble nucleation at the corroding surface, possible triggered by the release of strain during film cracking.

Temperature studies allowed the approximate determination of composite activation energies at 25 to 125 µm diameter Cu electrodes. Overall corrosion rates were obtained, consistent with a dominating effect of diffusion of poorly soluble copper species away from the electrode surface. Further work needs to be conducted to improve the understanding of these processes.

The observation that there is no significant underlying gas evolution even at very positive applied potentials allowed effects from gaseous species in the solution phase to be detected. Comparing the effects of vacuum-degassing and saturation with a range of gases (He, H_2, Ar, N_2, O_2, air, CO_2) showed that gases have a characteristic effect on the corrosion/passivation mechanism. CuCl film rupture and colloidal dissolution events increased in frequency in Ar- or CO_2-saturated electrolyte and were suppressed in degassed or He/H_2-treated electrolyte. This behaviour is consistent with the known effect of gases on water surface tension and on the related effects on gas bubble nucleation kinetics. O_2-saturation is proposed to affect the chemistry of the anodic corrosion process significantly, both in the initial stage of corrosion/passivation (CuCl formation) and throughout the corrosion process. It is proposed that oxygen reacts with the CuCl film, modifying the CuCl film mechanical properties, and leading to the formation of a more passive/stable film.

In some data sets, a more oscillatory/regular spike pattern is observed. Such observations could be linked also to local viscosity changes and/or Marangoni flow at the interface. There are further effects and phenomena that are not considered in this exploratory report. Further study will be needed to develop a better understanding of the noise component during the anodic corrosion of copper.

The link of gas bubble nucleation to passive film rupture could be more widely applicable for processes without intrinsic gas evolution. Bubble nucleation is linked to the ability of gases to act as surfactants by changing the surface tension of water. A range of distinct behaviours were observed from helium (which appears to suppress current spikes) to CO_2 (which appears to be current spike enhancing). Further study of these phenomena will be required.

Acknowledgements

We thank members of the Department of Chemistry, MC^2, and IMI at the University of Bath for ongoing support and access to facilities.

References

[1] T.E. Graedel, K. Nassau, J.P. Franey, Copper patinas formed in the atmosphere-I. Introduction, Corros Sci. 27 (1987) 639–649. doi:10.1016/0010-938X(87)90047-3.

[2] L. Nunez, E. Reguera, F. Corvo, E. Gonzalez, C. Vazquez, Corrosion of copper in seawater and its aerosols in a tropical island, Corros Sci. 47 (2005) 461–484. doi:10.1016/j.corsci.2004.05.015.

[3] G. Kear, B.D. Barker, F.C. Walsh, Electrochemical corrosion of unalloyed copper in chloride media − a critical review, Corros Sci. 46 (2004) 109–135. doi:10.1016/S0010-938X(02)00257-3.

[4] H. Cesiulis, N. Tsyntsaru, A. Ramanavicius, G. Ragoisha, The Study of Thin Films by Electrochemical Impedance Spectroscopy, in: I. Tiginyanu, P. Topala, V. Ursaki (Eds.), Nanostructures Thin Film Multifunct Appl Technol Prop Devices, Springer, Basel, 2016: pp. 3–43. doi:10.1007/978-3-319-30198-3.

[5] F. Arjmand, A. Adriaens, Influence of pH and chloride concentration on the corrosion behavior of unalloyed copper in NaCl solution: A comparative study between the micro and macro scales, Materials (Basel). 5 (2012) 2439–2464. doi:10.3390/ma5122439.

[6] E.J.J. Schindelholz, H. Cong, C.F.F. Jove-Colon, S. Li, J.A.A. Ohlhausen, H.K.K. Moffat, Electrochemical aspects of copper atmospheric corrosion in the presence of sodium chloride, Electrochim Acta. 276 (2018) 194–206. doi:10.1016/j.electacta.2018.04.184.

[7] S. Li, M.T. Teague, G.L. Doll, E.J. Schindelholz, H. Cong, Interfacial corrosion of copper in concentrated chloride solution and the formation of copper hydroxychloride, Corros Sci. 141

(2018) 243–254. doi:10.1016/j.corsci.2018.06.037.

[8] A.R. Langley, M. Carta, R. Malpass-Evans, N.B. McKeown, J.H.P. Dawes, E. Murphy, F. Marken, Linking the Cu(II/I) potential to the onset of dynamic phenomena at corroding copper microelectrodes immersed in aqueous 0.5 M NaCl, Electrochim Acta. 260 (2018) 348–357. doi:10.1016/j.electacta.2017.12.083.

[9] M. Drogowska, L. Brossard, H. Menard, Effects of Phosphate Ions on Copper Dissolution and Passivation, J Electrochem Soc. 139 (1992) 2787–2793. doi:10.1149/1.2068980.

[10] S. Aksu, Electrochemical Equilibria of Copper in Aqueous Phosphoric Acid Solutions, J Electrochem Soc. 156 (2009) C387–C394. doi:10.1149/1.3215996.

[11] M.M. Laz, R.M. Souto, S. González, R.C. Salvarezza, A.J. Arvia, The formation of anodic layers on annealed copper surfaces in phosphate − containing solutions at different pH, Electrochim Acta. 37 (1992) 655–663. doi:10.1016/0013-4686(92)80068-W.

[12] A. Nishikata, M. Itagaki, T. Tsuru, S. Haruyama, Passivation and its Stability on Copper in Alkaline Solutions Containing Carbonate and Chloride Ions, Corros Sci. 31 (1990) 287–292. doi:10.1016/0010-938X(90)90121-K.

[13] S. González, M. Pérez, M. Barrera, A.R. González Elipe, R.M. Souto, Mechanism of Copper Passivation in Aqueous Sodium Carbonate−Bicarbonate Solution Derived from Combined X-ray Photoelectron Spectroscopic and Electrochemical Data, J Phys Chem B. 102 (1998) 5483–5489. doi:10.1021/jp981069k.

[14] Y. Ein-Eli, E. Abelev, M. Auinat, D. Starosvetsky, Observation of Extended Copper Passivity in Carbonate Solutions and Its Future Application in Copper CMP, Electrochem Solid-State Lett. 8 (2005) B69–B71. doi:10.1149/1.2096432.

[15] M. Drogowska, L. Brossard, H. Menard, Anodic Copper Dissolution in the Presence of Cl − Ions at pH 12, Corrosion. 43 (1987) 549–552. doi:10.5006/1.3583899.

[16] C.H. Bonfiglio, H.C. Albaya, O.A. Cobo, The kinetics of the anodic dissolution of copper in acid chloride solutions, Corros Sci. 13 (1973) 717–724. doi:10.1016/S0010-938X(73)80010-1.

[17] R.K. Flatt, P.A. Brook, The Effects of Anion Concentration on Anodic Polarization or Copper, Zinc and Brass, Corros Sci. 11 (1971) 185–196. doi:10.1016/S0010-938X(71)80134-8.

[18] H.P. Lee, K. Nobe, Kinetics and Mechanisms of Cu Electrodissolution in Chloride Media, J Electrochem Soc. 133 (1986) 2035–2043. doi:10.1149/1.2108335.

[19] J.H. Wang, W.J. Zhai, Study on Cu Passivation Film's Forming Condition in HEDP Electrolyte with BTA and Chloride Ion, Appl Mech Mater. 274 (2013) 471–474. doi:10.4028/www.scientific.net/AMM.274.471.

[20] A. Xu, C. Dong, X. Wei, X. Li, D.D. Macdonald, DFT and photoelectrochemical studies of point

defects in passive films on copper, J Electroanal Chem. 834 (2019) 216–222. doi:10.1016/j.jelechem.2018.12.033.

[21] D. Kong, C. Dong, M. Zhao, X. Ni, C. Man, X. Li, Effect of chloride concentration on passive film properties on copper, Corros Eng Sci Technol Int J Corros Process Corros Control. 53 (2018) 122–130. doi:10.1080/1478422X.2017.1413160.

[22] D. Kong, C. Dong, X. Wei, C. Man, X. Lei, F. Mao, X. Li, Size matching effect between anion vacancies and halide ions in passive film breakdown on copper, Electrochim Acta. 292 (2018) 817–827. doi:10.1016/j.electacta.2018.10.004.

[23] H.P. Lee, K. Nobe, A.J. Pearlstein, Film Formation and Current Oscillations in the Electrodissolution of Copper in Acidic Chloride Media. I. Experimental Studies, J Electrochem Soc. 132 (1985) 1031–1037. doi:10.1149/1.2114309.

[24] J. Wojtowicz, Oscillatory Behavior in Electrochemical Systems, in: J.O. Bockris, E. Conway, B (Eds.), Mod Asp Electrochem, 8th ed., Springer, Boston, MA, 1972: pp. 47–120. doi:10.1007/978-1-4615-7440-8_2.

[25] W. Li, K. Nobe, A.J. Pearlstein, Electrodissolution Kinetics of Iron in Chloride Solutions, J Electrochem Soc. 140 (1993) 1642. doi:10.1016/0272-7714(88)90078-9.

[26] M.R. Bassett, J.L. Hudson, Shil'nikov Chaos during Copper Electrodissolution, J Phs Chem. 92 (1988) 6963–6966. doi:10.1021/j100335a025.

[27] M.R. Bassett, J.L. Hudson, The Oscillatory Electrodissolution of Copper in Acidic Chloride Solution, J Electrochem Soc. 137 (1990) 1815–1826. doi:10.1149/1.2086580.

[28] M.R. Bassett, J.L. Hudson, The Dynamics of the Electrodissolution of Copper, Chem Eng Commun. 60 (1987) 145–159. doi:10.1080/00986448708912014.

[29] Q. Cui, H.D. Dewald, Current oscillations during copper electrodissolution under solution sparging in acidic NaCl solutions, Microchem J. 86 (2007) 80–88. doi:10.1016/j.microc.2006.11.003.

[30] H.D. Dewald, P. Parmananda, R.W. Rollins, Periodic and Chaotic Current Oscillations at a Copper Electrode in an Acetate Electrolyte, J Electrochem Soc. 140 (1993) 1969–1973. doi:10.1149/1.2220747.

[31] F.N. Albahadily, M. Schell, An experimental investigation of periodic and chaotic electrochemical oscillations in the anodic dissolution of copper in phosphoric acid, J Chem Phys. 88 (1998) 4312–4319. doi:10.1063/1.453790.

[32] C. Yi, Study on the Initial Atmospheric Corrosion Behavior of Copper in Chloride-Containing Environments, Int J Electrochem Sci. 12 (2017) 3597–3613. doi:10.20964/2017.05.18.

[33] A. V. Benedetti, P.T.A. Sumodjo, K. Nobe, P.L. Cabot, G.W. Proud, Electrochemical studies of

copper, copper-aluminium and copper-aluminium-silver alloys: impedance results in 0.5 M NaCl, Electrochim Acta. 40 (1995) 2657–2668. doi:10.1016/0013-4686(95)00108-Q.

[34] R. Massoudi, A.D. King, Effect of pressure on the surface tension of water. Adsorption of low molecular weight gases on water at 25.deg., J Phys Chem. 78 (1974) 2262–2266. doi:10.1021/j100615a017.

[35] M.A.J. Van Limbeek, J.R.T. Seddon, Surface nanobubbles as a function of gas type, Langmuir. 27 (2011) 8694–8699. doi:10.1021/la2005387.

[36] W.D. Weatherford, Homogeneous nucleation of gas bubbles in liquids, J Colloid Interface Sci. 34 (1970) 197–204. doi:10.1016/0021-9797(70)90169-4.

[37] S. Wildeman, H. Lhuissier, C. Sun, D. Lohse, A. Prosperetti, Tribonucleation of bubbles, in: Proc Natl Acad Sci, 2014: pp. 10089–10094. doi:10.1073/pnas.1321194111.

[38] H. Lal, H.R. Thirsk, The Anodic Behaviour of Copper in Neutral and Alkaline Chloride Solutions., J Chem Soc. (1953) 2638–2644. doi:10.1039/JR9530002638.

[39] D. Starosvetsky, O. Khaselev, M. Auinat, Y. Ein-Eli, Initiation of copper dissolution in sodium chloride electrolytes, Electrochim Acta. 51 (2006) 5660–5668. doi:10.1016/j.electacta.2006.01.058.

[40] P. Atkins, J. De Paula, The Properties of Gases, in: Atkins' Phys Chem, 9th ed., Oxford University Press, Oxford, 2010: p. 28.

[41] D.R. Lide, ed., CRC Handbook of Chemistry and Physics, 74th ed., CRC Press, Inc, 1993.

[42] L. Korson, W. Drost-Hansen, F.J. Millero, Viscosity of water at various temperatures, J Phys Chem. 73 (1969) 34–39. doi:10.1021/j100721a006.

[43] R.C. Hamme, S.R. Emerson, The solubility of neon, nitrogen and argon in distilled water and seawater, Deep Res Part I Oceanogr Res Pap. 51 (2004) 1517–1528. doi:10.1016/j.dsr.2004.06.009.

[44] F. Qiu, R.G. Compton, B.A. Coles, F. Marken, Thermal activation of electrochemical processes in a Rf-heated channel flow cell: Experiment and finite element simulation, J Electroanal Chem. 492 (2000) 150–155. doi:10.1016/S0022-0728(00)00222-9.

[45] S.J. Kim, M. Okido, K.M. Moon, An electrochemical study of cathodic protection of steel used for marine structures, Korean J Chem Eng. 20 (2003) 560–565. doi:10.1007/BF02705566.

[46] Y. Bai, Q. Bai, Subsea Corrosion and Scale, in: Subsea Eng Handb, 2010: pp. 505–540. doi:10.1016/B978-1-85617-689-7.10017-2.

[47] M. Piri, R. Arefinia, Investigation of the hydrogen evolution phenomenon on CaCO3precipitation in artificial seawater, Desalination. 444 (2018) 142–150. doi:10.1016/j.desal.2018.05.018.

[48] S.D. Lubetkin, Why is it much easier to nucleate gas bubbles than theory predicts?, Langmuir. 19

(2003) 2575–2587. doi:10.1021/la0266381.

[49] S. Lubetkin, M. Blackwell, The nucleation of bubbles in supersaturated solutions, J Colloid Interface Sci. 126 (1988) 610–615. doi:10.1016/0021-9797(88)90161-0.

[50] G. Bianchi, P. Longhi, Copper in sea-water, potential-pH diagrams, Corros Sci. 13 (1973) 853–864. doi:10.1016/S0010-938X(73)80067-8.

[51] C. Young-Gab, P. Su-Il, K. Chang-Ha, Effect of aluminium content on the anodic behaviour of copper-aluminium alloys in 3.5 wt% NaCl solution, Mater Lett. 20 (1994) 265–270. doi:10.1016/0167-577X(94)90027-2.

[52] F. Mansfeld, G. Liu, H. Xiao, C.H. Tsai, B.J. Little, The corrosion behavior of copper alloys, stainless steels and titanium in seawater, Corros Sci. 36 (1994) 2063–2095. doi:10.1016/0010-938X(94)90008-6.

[53] M.M. Al-Abdallah, A.K. Maayta, M.A. Al-Qudah, N.A.F. Al-Rawashdeh, Corrosion Behavior of Copper in Chloride Media, Open Corros J. 2 (2009) 71–76. doi:10.2174/1876503300902010071.

[54] B. Yin, S. Zhang, X. Zheng, F. Qu, X. Wu, Cuprous Chloride Nanocubes Grown on Copper Foil for Pseudocapacitor Electrodes, Nano-Micro Lett. 6 (2014) 340–346. doi:10.1007/s40820-014-0007-3.

[55] C. Deslouis, B. Tribollet, G. Mengoli, M.M. Musiani, Electrochemical behaviour of copper in neutral aerated chloride solution. I. Steady-state investigation, J Appl Electrochem. 18 (1988) 374–383. doi:10.1007/BF01093751.